

# **Mono and biallelic variants in *HCN2* cause severe neurodevelopmental disorders**

Clara Houdayer<sup>1†‡</sup>, A Marie Phillips<sup>2,3,†</sup>, Marie Chabbert<sup>4</sup>, Jennifer Bourreau<sup>4</sup>, Reza Maroofian<sup>5</sup>, Henry Houlden<sup>5</sup>, Kay Richards<sup>2</sup>, Nebal Waill Saadi<sup>6</sup>, Eliška Dad'ová<sup>4</sup>, Patrick Van Bogaert<sup>7</sup>, Mailys Rupin<sup>7</sup>, Boris Keren<sup>8</sup>, Perrine Charles<sup>8</sup>, Thomas Smol<sup>9</sup>, Audrey Riquet<sup>10</sup>, Lynn Pais<sup>11,12</sup>, Anne O'Donnell-Luria<sup>11,12</sup>, Grace E. VanNoy<sup>11</sup>, Allan Bayat<sup>13,14</sup>, Rikke S Møller<sup>13,14</sup>, Kern Olofsson<sup>15</sup>, Rami Abou Jamra<sup>16</sup>, Steffen Syrbe<sup>17</sup>, Majed Dasouki<sup>18</sup>, Laurie H Seaver<sup>19,20</sup>, Jennifer A Sullivan<sup>21</sup>, Vandana Shashi<sup>21</sup>, Fowzan S Alkuraya<sup>22</sup>, Alexis F Poss<sup>23</sup>, J Edward Spence<sup>23</sup>, Rhonda E Schnur<sup>24</sup>, Ian C Forster<sup>2</sup>, Chaseley E Mckenzie<sup>2</sup>, Cas Simons<sup>25</sup>, Min Wang<sup>25</sup>, Penny Snell<sup>25</sup>, Kavitha Kothur<sup>26</sup>, Michael Buckley<sup>27</sup>, Tony Roscioli<sup>27</sup>, Noha Elserafy<sup>27</sup>, Benjamin Dauriat<sup>28</sup>, Vincent Procaccio<sup>1,29</sup>, Daniel Henrion<sup>4</sup>, Guy Lenaers<sup>1,29</sup>, Estelle Colin<sup>1,29</sup>, Nienke E. Verbeek<sup>30</sup>, Koen L. Van Gassen<sup>30</sup>, Claire Legendre<sup>4</sup>, Dominique Bonneau<sup>1,29</sup>, Christopher A Reid<sup>2</sup>, Katherine B Howell<sup>25,31</sup>, Alban Ziegler<sup>1,29,32†</sup>, Christian Legros<sup>4†‡</sup>

**†These authors contributed equally to this work.**

**‡Co-corresponding authors.**

## Abstract

Hyperpolarization activated Cyclic Nucleotide (HCN) gated channels are crucial for various neurophysiological functions, including learning and sensory functions, and their dysfunction are responsible for brain disorders, such as epilepsy. To date, *HCN2* variants have only been associated with mild epilepsy and recently, one monoallelic missense variant has been linked to developmental and epileptic encephalopathy. Here, we expand the phenotypic spectrum of *HCN2*-related disorders by describing twenty-one additional individuals from fifteen unrelated families carrying *HCN2* variants. Seventeen individuals had developmental delay/intellectual disability (DD/ID), two had borderline DD/ID, and one had borderline DD. Ten individuals had epilepsy with DD/ID, with median age of onset of 10 months, and one had epilepsy with normal development. Molecular diagnosis identified thirteen different pathogenic *HCN2* variants, including eleven missense variants affecting highly conserved amino acids, one frameshift variant, and one in-frame deletion. Seven variants were monoallelic of which five occurred *de novo*, one was not maternally inherited, one was inherited from a father with mild learning disabilities, and one was of unknown inheritance. The remaining six variants were biallelic, with four homozygous and two compound heterozygous variants. Functional studies using two-electrode voltage-clamp recordings in *Xenopus laevis* oocytes were performed on three monoallelic variants, p.(Arg324His), p.(Ala363Val), and p.(Met374Leu), and three biallelic variants, p.(Leu377His), p.(Pro493Leu) and p.(Gly587Asp). The p.(Arg324His) variant induced a strong increase of HCN2 conductance, while p.(Ala363Val) and p.(Met374Leu) displayed dominant negative effects, leading to a partial loss of HCN2 channel function. By confocal imaging, we found that the p.(Leu377His), p.(Pro493Leu) and p.(Gly587Asp) pathogenic variants impaired membrane trafficking, resulting in a complete loss of HCN2 elicited

currents in *Xenopus* oocytes. Structural 3D-analysis in depolarized and hyperpolarized states of HCN2 channels, revealed that the pathogenic variants p.(His205Gln), p.(Ser409Leu), p.(Arg324Cys), p.(Asn369Ser) and p.(Gly460Asp) modify molecular interactions altering HCN2 function. Taken together, our data broadens the clinical spectrum associated with *HCN2* variants, and disclose that *HCN2* is involved in developmental encephalopathy with or without epilepsy.

**Author affiliations:**

1. Department of Medical Genetics, Angers University Hospital, 49933 Angers, France.
2. Florey Institute of Neuroscience and Mental Health, The University of Melbourne, Parkville Vic, Australia.
3. School of Biosciences, The University of Melbourne, Parkville, VIC, Australia.
4. Univ Angers, INSERM, CNRS, MITOVASC, Equipe CarMe, SFR ICAT, F-49000 Angers, France.
5. Department of Neuromuscular Disorders, UCL Queen Square Institute of Neurology, University College London, London, United Kingdom.
6. College of Medicine, University of Baghdad, Baghdad 10001, Iraq; Children Welfare Teaching Hospital, Medical City Complex, Baghdad 10001, Iraq.
7. Department of Pediatric Neurology, Angers University Hospital, 49933 Angers, France.
8. Department of Genetics, Pitié-Salpêtrière Hospital, Assistance Publique-Hôpitaux de Paris, 75019 Paris, Sorbonne University, France.

9. Univ. Lille, CHU Lille, ULR7364 – RADEME, Institute of Medical Genetics, F-59000 Lille, France.

10. Department of Pediatric Neurology, Saint Vincent de Paul Hospital, GHICL, Lille, France.

11. Program in Medical and Population Genetics, Broad Institute of MIT and Harvard, Cambridge, MA, USA.

12. Division of Genetics and Genomics, Boston Children's Hospital, Boston, MA, USA.

13. Department for genetics and personalized medicine, Danish Epilepsy Centre, Dianalund, Denmark.

14. Department Regional Health Research, University of Southern Denmark, Odense, Denmark.

15. Department of Paediatrics, Danish Epilepsy Centre Filadelfia, 4293 Dianalund, Denmark.

16. Institute of Human Genetics, University of Leipzig Medical Center, Germany.

17. Division of Paediatric Epileptology, Centre for Paediatrics and Adolescent Medicine, University Hospital Heidelberg, Heidelberg, Germany.

18. Department of Medical Genetics, Genomics and Personalized Health at AdventHealth-Orlando, Florida, USA.

19. Division of Medical Genetics, Corewell Health Helen DeVos Children's Hospital, Grand Rapids, MI, 49503, USA.

20. Department of Pediatrics and Human Development, Michigan State University College of Human Medicine, Grand Rapids, MI, 49503, USA.

21. Department of Pediatrics-Medical Genetics, Duke University, Durham, NC 27710, USA.
22. Department of Translational Genomics, Center for Genomic Medicine, King Faisal Specialist Hospital & Research Center, Riyadh, Saudi Arabia.
23. Pediatrics-Clinical Genetics and Metabolism, School of Medicine, University of Colorado-Anschutz Medical Campus, Aurora, Colorado, USA.
24. GeneDx, Gaithersburg, MD 20877, USA.
25. Murdoch Children's Research Institute, Melbourne, Australia.
26. Department of Neuropediatrics, The Children's Hospital at Westmead, Sydney Children's Hospital Network, Sydney, Australia.
27. New South Wales Health Pathology Randwick Genomics Laboratory, Sydney, NSW, Australia.
28. Department of Medical Genetics and Cytogenetics, Limoges University Hospital, France
29. Univ Angers, INSERM, CNRS, MITOVASC, Equipe MitoLab, SFR ICAT, F-49000 Angers, France.
30. Department of Genetics, University Medical Center Utrecht, Utrecht, The Netherlands.
31. Department of Neurology, Royal Children's Hospital, Melbourne, Australia.
32. Department of Medical Genetics, University Hospital of Reims, Reims, France

Correspondence to: Clara Houdayer and Christian Legros

4 rue Larrey - 49 933 Angers Cedex 9

clara.houdayer@chu-angers.fr

christian.legros@univ-angers.fr

**Running title:** Expanding *HCN2* variants phenotypic spectrum

**Keywords:** HCN2, Hyperpolarization activated cyclic nucleotide gated channel 2; channelopathies; epileptic encephalopathy; neurodevelopmental disorder; two-electrode voltage-clamp.

**Abbreviations:**

AA = amino-acid; CNBD = cyclic nucleotide-binding domain; DEE = developmental and epileptic encephalopathy; EE-SWAS= epileptic encephalopathy with spike-wave activation in sleep; FS= febrile seizures; GEFS = generalized epilepsy with febrile seizures; GGE = genetic generalized epilepsy; GOF = gain-of-function; HCN = hyperpolarization activated cyclic nucleotide gated channel;  $I_{\max}$  = maximal current; ID = intellectual disability; LOF = loss-of-function; SOS = standard oocyte saline; TEVC = two-electrode voltage-clamp method; wt-HCN2 = wild-type HCN2.

## Introduction

Diseases resulting from dysfunction of ion channels, collectively known as channelopathies, often manifest as neurodevelopmental disorders associated with epilepsy.<sup>1-3</sup> Among the ion channels involved in epilepsy, the Hyperpolarization activated Cyclic Nucleotide (HCN) gated ion channels, have been highlighted as important regulators of neuronal excitability in disease for more than two decades.<sup>4-7</sup> The human genome contains four distinct HCN genes (*HCN1-4*) that have a high level of sequence homology, but exhibit different cerebral expression patterns. *HCN1* and *HCN2* are the most abundant and widely expressed isoforms

in brain, while *HCN3* is predominant in the cerebellum, and *HCN4* is weakly expressed in the brain but highly abundant in the heart.<sup>4,8</sup>

HCN 1-4 channels are composed of four subunits forming a central ion-conducting pore and assembled in homo- or heterotetramers.<sup>9</sup> Their structure-function relationships have been extensively investigated,<sup>10</sup> and the cryo-EM structure of the human HCN1 channel has provided insight into the gating and ion selectivity mechanisms at the molecular level.<sup>11</sup> HCN1-4 channels open upon hyperpolarization of the membrane to generate a Na<sup>+</sup> inward current, called I<sub>h</sub> and I<sub>f</sub> in neurons<sup>12,13</sup> and cardiomyocytes<sup>14,15</sup> respectively, leading to membrane depolarization in excitable cells and exhibiting pacemaker activity. These ion channels are potentiated by intracellular cyclic monophosphate nucleotides cAMP and cGMP, through a positive shift of activation range.<sup>4,16</sup> The I<sub>h</sub> current is involved in resting potential regulation, dendritic integration, and synaptic transmission.<sup>4</sup> Several studies performed on transgenic mice have established a relationship between *HCN1* and *HCN2* and neuronal excitability and epileptogenesis, and being implicated in various neurophysiological processes, including sleep, learning, memory, and sensory functions.<sup>17-20</sup>

Of the HCN channels, HCN1 has been extensively investigated in human neurological disease. Heterozygous missense *HCN1* variants were first reported in individuals with developmental and epileptic encephalopathy (DEE) (DEE24; # 615871).<sup>21-23</sup> Thereafter, *HCN1* has been associated with a broader clinical spectrum including febrile seizures, milder epilepsies (including genetic generalized epilepsies (GGE) and genetic epilepsy with febrile seizures plus (GEFS+)), and intellectual disability (ID) without seizures.<sup>23</sup> A genotype/phenotype correlation has been identified, with *HCN1* variants located in the transmembrane domain being associated with DEE, while those located in the N- or C-terminal mostly resulted in milder epilepsy.<sup>23</sup>

To date, six pathogenic *HCN2* variants have been reported in a restricted number of individuals, with mild epilepsies including GGE and GEFS+, mostly without ID (Table 1, Fig. 1A).<sup>24-27</sup> Only two individuals with *HCN2* variants had ID: one of the three individuals from the family carrying the p.(Val246Met) variant, and one girl presenting ID and epilepsy, caused by a *de novo* p.(Gly460Asp) variant.<sup>27,28</sup> Electrophysiological studies have revealed that most *HCN2* variants studied to date p.(Pro719-Pro721del) (previously reported as delPPP), p.(Ser632Trp) and p.(Val246Met) produce a gain-of-function (GOF) of the HCN2 channel, due to either larger current densities, faster kinetics, or a positive shift of voltage-dependent activation.<sup>27,29</sup> The biallelic p.(Glu515Lys) and the monoallelic p.(Gly460Asp) variants have been reported to cause loss-of-function (LOF); the first, by slowing activation kinetics and shifting activation to more hyperpolarized potentials, resulting in an absence of current<sup>25</sup> and the second, by inducing a strong reduction of the current density secondary due to trafficking defect to the cell membrane.<sup>28</sup>

In this study, we report twenty-one individuals from fifteen unrelated families, carrying twelve novel mono- or biallelic *HCN2* variants. By characterizing the biophysical properties of six variants by two-electrode voltage-clamp method (TEVC), Western blot analysis and 3D modeling, we demonstrate that *HCN2* variants are associated with a more severe and broader clinical spectrum of neurodevelopmental disorders than previously reported, and confirm its involvement in DEE.



## **Materials and methods**

### **Individual recruitment and clinical phenotyping**

This study was performed in accordance with ethical principles for medical research outlined in the Declaration of Helsinki. Individuals harboring *HCN2* pathogenic or likely pathogenic variants were recruited through an international collaborative effort facilitated by GeneMatcher<sup>30</sup>. Consents for publication of clinical data including genetic analyses were obtained from all individuals or their parents.

Individuals were enrolled from epilepsy and genetic centers located in Australia, Denmark, France, Germany, Netherlands, Saudi Arabia, UK, and USA. Physicians recorded clinical, EEG, neuroimaging and genetic data using a dedicated form. Epilepsy syndromes and seizure type were classified according to the International League Against Epilepsy (ILAE) guidelines.<sup>31</sup>

### **Genetic analysis**

Genetic analyses were performed in a diagnostic or research laboratory in all individuals, and when available, in their parents. *HCN2* variants were identified using either proband-only or Trio-exome or genome sequencing and confirmed by Sanger sequencing. Variants were classified according to ACMG criteria.<sup>32</sup> The consequences of *HCN2* variants were interpreted on isoform NM\_001194.4 (Supplementary Table 1).

### ***TEVC recording of wt-HCN 2 and its variants.***

### ***HCN2* mutagenesis and *in vitro* transcription**

A synthetic wild-type HCN2 cDNA (Genecust, Boynes, France) corresponding to the coding wild-type sequence of *HCN2* (wt-HCN2) (NM\_001194.4) was inserted between the *Bam*HI and *Hind*III sites in pGEM-HEJUEL, an expression vector suitable for *Xenopus laevis* oocyte expression. The *HCN2* variants, p.(Arg324His), p.(Ala363Val), p.(Met374Leu), p.(Leu377His), p.(Pro493Leu) and p.(Gly587Asp), were generated by site-mutagenesis, and their sequences were verified by Sanger sequencing. mRNAs were prepared from linearized cDNA templates by *in vitro* transcription using the mMACHINE mMESSAGE mMACHINE® T7 transcription Kit (Ambion, Fisher Scientific S.A.S., Illkirch, France) and purified with the NucleoSpin RNA clean up kits (Macherey Nagel, Düren, Germany) or RNeasyPlus (Qiagen, Germany) and quantified by nanospectrophotometry and stored at -24°C or -80°C until used.

### **Oocyte preparation and mRNA injection**

All animal procedures were performed in accordance with the European Community council directive 2010/63/EU for the care and use of laboratory animals, and approved by the French Ministry of Agriculture (authorization N°A49007002 and APAFIS N#19433-2019022511329240v2). The NC3R's ARRIVE guidelines were followed in the conduct of all experiments using animals. Adult *Xenopus laevis* females were used for oocytes collection as previously described.<sup>33,34</sup> For HCN2 expression, 21 ng of mRNA (wt-HCN2 or its variants) were injected into individual defolliculated oocytes, using an automatic nanoinjector (Nanoject II Drummond Scientific) or the Roboinject (Multi Channel Systems, Reutlingen, Germany). To mimic heterozygosity, heterotetrameric channels (e.g. wt/p.(Arg324His)) were produced by co-expression experiments with equal amounts (10.5 ng) of wt-*HCN2* and *HCN2* variant mRNAs. Injected oocytes were incubated 3-4 days at 18°C prior TEVC recordings.

## **Two-Electrode Voltage Clamp Recording**

Details of solutions used for TEVC recordings can be found in the Supplementary material. Non-injected oocytes were used as negative control. From a holding potential,  $V_h = -30$  mV, currents were elicited with a two-step protocol, comprising: i) an activation step in 10 mV increments from -140 mV to -30 mV for 8 s and ii) a return to -130 mV for 3 s. The first step of this protocol was used to establish the current-voltage relationships after current densities calculation with membrane capacitance. The second step was used to characterize the voltage-dependency of activation after normalization with maximum current amplitude. Currents were analysed using Clampfit 10.7 (Molecular Devices).

## **Western blot analysis**

Details of solutions and Western blotting procedures are available in the Supplementary material. Thirty  $\mu$ g of protein from control and experimental samples (equivalent to protein from 80%-100% of protein from one oocyte) were separated by electrophoresis on 8% polyacrylamide SDS-PAGE gels. Proteins were transferred to nitrocellulose and blots were blocked with a milk-containing solution before incubation with 1:500 rabbit anti-HCN2 APC-030 (Alomone Labs Cat# APC-030, RRID: AB2313726). Beta-actin (Thermo Fisher Scientific Cat# PA1-183, RRID:AB\_2539914) was used as a loading control. The protein signal was visualized with Clarity Western ECL Substrate (Bio-Rad, CA, USA) and the signal captured by a Bio-Rad ChemiDoc™ MP imaging system (Image Lab Software, RRID: SCR\_014210).

## **Transient expression in HEK293 cells and confocal fluorescent microscopy**

Details of solutions and procedure are available in the Supplementary material. HEK293T cells were transfected with N-terminal EGFP tagged constructs encoding human wt-HCN2,

p.(Leu377His), p.(Pro493Leu) and p.(Gly587Asp). As negative control, a truncated HCN2<sub>ΔC-X</sub> (Thr553Ter), a trafficking-deficient construct, was used.<sup>35</sup> The membrane was labelled with CellMask Orange Plasma Membrane. The nuclei were stained with DAPI. Images were collected at 20x overview and then at high resolution (magnification objective: 63x) using Airy scan. The imager was “blind” to the genotype of the constructs.

### **Protein 3D modelling and structural analysis**

Molecular models of depolarized and hyperpolarized wild type HCN2 were built with MODELLER V9.17 from position 163, by homology with the cryo-electron microscopy of human HCN1 (PDB 5U6P and 6UQF corresponding to depolarized and hyperpolarized models, respectively) (Supplementary Fig. 1).<sup>11,36</sup> These templates were selected after comparison with rabbit HCN4 (PDB 7NMN).<sup>37</sup> HCN1 and HCN4 structures differ in the S4-S5 linker, with an Mg<sup>2+</sup> binding site observed only in HCN4.<sup>38</sup> For each modelling, twenty structures were built and refined by simulated annealing (refine.fast option). The final models were selected according to the MODELLER PDFf score. The wt-HCN2 3D-models were subsequently used as templates for modeling the p.(His205Gln), p.(Arg324His), p.(Arg324Cys), p.(Ala363Val), p.(Asn369Ser), p.(Met374Leu), p.(Leu377His), p.(Gly460Asp), p.(Glu478del), p.(Pro493Leu) and p.(Gly587Asp) variants, in resting and hyperpolarized states. The 3D-models were graphically inspected with PyMOL (Molecular Graphics System, version 1.8, Schrödinger, LLC) to analyse the impact of each variant on HCN2 structure. The solvent accessible surface area (ASA) and the relative solvent accessibility (RSA) were calculated with PyMOL with a solvent radius of 1.4 Å. HCN2 structures were also analysed using two predictive and analytical tools developed by Biosig Lab available at <https://biosig.lab.uq.edu.au/>. The tools called DDMut (<https://biosig.lab.uq.edu.au/ddmut/>) and DynaMut (<https://biosig.lab.uq.edu.au/dynamut/>)

were used to compute the Gibbs free energy ( $\Delta\Delta G$ )  $\Delta$  vibrational entropy energy between wt-HCN2 and variant ( $\Delta\Delta S_{Vib}$  ENCoM), giving information on structure flexibility.<sup>39,40</sup>

### **Graphs and statistical analysis**

All graphs and statistical analyses were performed using GraphPad Prism 7.02 software (La Jolla, CA, USA). Data are mean  $\pm$  standard error of the mean (SEM). The normality of sample distribution was assessed with the Shapiro-wilk test and, as appropriate, differences between groups were analysed with parametric or nonparametric tests, as indicated in the legends of the figures. The significance of the tests was considered for the following conditions:  $P < 0.05$  (\*),  $P < 0.01$  (\*\*),  $P < 0.001$  (\*\*\*) and  $P < 0.0001$  (\*\*\*\*).

### **Data availability**

Supporting data for the results of this study are available from the corresponding authors [CH, CL], upon reasonable request.

## **Results**

### **Clinical characteristics of *HCN2*-related neurodevelopmental disorders**

The clinical data of the twenty-one individuals (11 females, 10 males) reported here, whose ages ranged from 2 to 61 years (median age 8 years and 2 month), are summarized in Table 2. Developmental delay (DD/ID) was present in 17/21 individuals, and was of variable severity: mild (3/17, 18%), moderate (3/17, 18%), severe to profound (10/17, 59%), unspecified (1/17, 6%). Developmental regression was reported in four individuals, and was temporally related to epilepsy in one.

Twelve individuals (57%) had seizures, two having febrile seizures (FS) only and ten (48%) having epilepsy. The median age of epilepsy onset was 10 months (range 1 month - 6 years). A range of seizure types and EEG patterns were observed. One individual had infantile epileptic spasms syndrome, one had epileptic encephalopathy with spike-wave activation in sleep (EE-SWAS), and the remaining patients had unclassified epilepsies. No consistent treatment response was identified. Seizures were ongoing at last review in 3/10 individuals.

Tone abnormalities (hypo- or hypertonia) were present in sixteen individuals (76%) (Table 2). Ten individuals had movement disorders, including dystonia (n = 6), stereotypies (n = 5), static cerebellar signs (n = 1) and tremor (n = 2). Nystagmus was present in eight individuals (38%). Thirteen individuals (I1,I9-I11, I20-21) exhibited normal brain MRI. Abnormal brain MRI were observed for 9 individuals (I2, I5-8, I13-15, and I19). Brain MRI showed periventricular white matter T2 hyperintensities in five individuals, including the three carrying the p.(Glu478del) variant (Table 3, Supplementary Fig. 2).

## **Identification of monoallelic and biallelic variants in *HCN2***

We identified thirteen different variants in the coding sequence of *HCN2*, twelve were novel, including eleven missense variants, one recurrent in-frame deletion (I13-15), one frameshift variant. The distribution of the *HCN2* variants along the protein sequence is shown in Fig. 1A. Among these variants, seven were monoallelic including five *de novo*, one not maternally inherited and one inherited over three generations (Fig. 1B). The remaining six variants were biallelic including four homozygous and two compound heterozygous. Noteworthy, the compound heterozygous variants resulted

from the unusual combination of one *de novo* variant (p.(Ser409Leu)) and one variant in trans (p.(His205Gln)), inherited from the asymptomatic mother. The p.(Glu478del) variant was found recurrently in three unrelated individuals, and two variants, namely p.(Arg324Cys) and p.(Arg324His), involved the same amino acid (AA). The p.(Gly460Asp) variant was previously described as a DEE causing variant.<sup>28</sup> All thirteen variants have *in silico* prediction scores in favour of a deleterious effect. They all affect an AA that is highly conserved across all HCN subtypes in humans and other species (Fig. 1B), and are absent or extremely rare in the gnomAD database (Supplementary Table 1). Moreover, they all are clustered in the S4-S5 segments, the C-linker and the CNBD with no obvious correlation with the mode of inheritance.

### **Electrophysiological studies of the monoallelic variants, p.(Arg324His), p.(Ala363Val) and p.(Met374Leu)**

Next, we characterized three monoallelic variants by TEVC: p.(Arg324His), located in S4, and p.(Ala363Val), and p.(Met374Leu), located in S5 (Fig. 1A). With control non-injected oocytes, the observed currents were rectangular, strictly proportional to the stimulation intensity and did not exceed  $0.72 \pm 0.10$  nA/nF (maximal current density at  $V_m = -130$  mV,  $n = 10$ ), indicating the absence of voltage-gated endogenous currents activated by the voltage step stimulation protocol (Fig. 2A, B). The current families generated by the wt/p.(Arg324His) variant appeared similar in shape to that of wt-HCN2, but with much larger amplitudes (Fig. 2A). In contrast, the current families of wt/p.(Ala363Val), and wt/p.(Met374Leu) mixtures exhibited smaller amplitudes and different patterns (Fig. 2A). HCN2 currents exhibited three parts: an instantaneous step, a slowly activating phase that reaches a steady-state (Fig. 2A), as already described.<sup>41</sup>

To characterize the impact p.(Arg324His), p.(Ala363Val) and p.(Met374Leu) variants, we compared the current densities of these three components with those elicited by wt-HCN2. Concerning wt/p.(Arg324His), the current densities of steady-state, instantaneous and slow components were significantly higher (3 to 5-fold) than those of wt-HCN2 from -130 to -70 mV (Fig. 2B). Concerning wt/p.(Ala363Val) and wt/p.(Met374Leu) combinations, we observed profound modifications of current shape in comparison with wt-HCN2 (Fig. 2A). The instantaneous components elicited by these two variants were similar to those of wt-HCN2 (Fig. 2C and D, middle graphs). The wt/p.(Ala363Val) variant elicited significantly lower current densities for both steady-state and slow components than wt-HCN2 from -130 to -80 mV (Fig. 2C, left and right graphs). For the p.(Met374Leu) variant, we observed lower current densities of the slow component only (Fig. 2D, right graph). Then, wt/p.(Ala363Val) and wt/p.(Met374Leu) variants induced a five and three-fold decrease of the slow component of HCN2 currents, respectively. The Western blots did not show any obvious significant protein reduction for either variant (Supplementary Fig. 3).

The slow component of wt-HCN2 and wt/p.(Arg324His) current traces could be best-fitted with a two exponential equation, whereas those of both wt/p.(Ala363Val) and wt/p.(Met374Leu) variants were best fitted with a mono-exponential equation, which was therefore used to analyse all traces (Fig. 3A). The current traces of p.(Arg324His) variant exhibited slightly faster activation kinetics only from -130 to -110 mV ( $P < 0.05$ , Fig. 3B, left graph). For both wt/p.(Ala363Val) and wt/p.(Met374Leu) variants, we observed a significant increase in the rate of activation from -130 mV to -80 mV than of wt-HCN2, which was all the more important as  $V_m$  was positive (Fig. 3B, middle and right graphs).



Next, we analysed the instantaneous tail currents that correspond to activation phase, using the Boltzmann equation (Fig. 3C). The data were well fitted, allowing the determination of the half potential of activation ( $V_{1/2}$ ) and the slope coefficients ( $k$ ). With wt/p.(Arg324His) channel, the  $V_{1/2}$  and  $k$ -values were not significantly different from those of wt-HCN2 channel (Fig. 3D). In contrast, with both wt/p.(Ala363Val) and wt/p.(Met374Leu) channels,  $V_{1/2}$  of activation were shifted to the left by 60.8 and 43.0 mV, respectively ( $P < 0.0001$ , Fig. 4D). This hyperpolarized shift was significantly larger for p.(Ala363Val) variant than p.(Met374Leu) variant ( $P < 0.0001$ , Fig. 3D, middle graph). For these two variants, the slopes were significantly shallower than that of wt-HCN2 ( $P < 0.0001$ , Fig. 3D, right graph).

Taken together, our electrophysiological data show that the p.(Arg324His) variant results in GOF, whereas the p.(Ala363Val) and p.(Met374Leu) variants induce a partial LOF, when they are expressed in *Xenopus* oocytes.

## **Electrophysiological, Western blot and immunocytochemical analyses of the biallelic variants, p.(Leu377His), p.(Pro493Leu) and (Gly587Asp)**

The biallelic variants p.(Leu377His), p.(Pro493Leu) and p.(Gly587Asp), were then individually expressed in *Xenopus* oocytes to investigate their functional impact on HCN2. The data from expression experiments of p.(Leu377His), p.(Pro493Leu) and p.(Gly587Asp) are shown in Fig. 4. Neither p.(Leu377His) ( $n = 8$ ), p.(Pro493Leu) ( $n = 6$ ) nor p.(Gly587Asp) ( $n = 4$ ) produced any measurable currents (Fig. 4A, C and E). Western blot showed a strong immunoreactivity for two bands with apparent molecular weight close to 100 kDa with wt-HCN2 (Fig. 4B, D and F). These two bands

likely reflect a glycosylated and a non-glycosylated form of wt-HCN2.<sup>38</sup> However, p.(Leu377His) and p.(Pro493Leu) showed only one band corresponding to the non-glycosylated form, while p(Gly587Asp) variant behaved as wt-HCN2. We hypothesized that the LOF of these three *HCN2* variants could be the consequence of the alteration of membrane trafficking. We addressed this question by expressing p.(Leu377His), p.(Pro493Leu) and p(Gly587Asp) variants tagged with EGFP in HEK293 cells and imaging their trafficking to the plasma membrane by confocal microscopy (Fig. 4G-J). While EGFP-tagged wt-HCN2 showed staining of the plasma membrane (Fig. 4G), no obvious membrane expression was observed for p.(Leu377His), p.(Pro493Leu) and p(Gly587Asp) variants (Fig. 4H-J). Indeed, a strong EGFP-staining of cytosol was observed, indicating that all biallelic variants remain in the cytosol. In conclusion, these data evidence that the biallelic p.(Leu377His), p.(Pro493Leu) and p.(Gly587Asp) variants induce a complete LOF, due to the impairment of membrane trafficking.

## **Structural Impacts of the identified pathogenic variants onto a 3D Homology model of HCN2**

Next, we built 3D homology models of the HCN2 channel to further investigate the structural impact of all variants reported in this work (Fig. 5). We thus examined each mutation in both depolarized and hyperpolarized states. We first examined the effects of each missense mutation on HCN2 structure stability, by analysing the  $\Delta\Delta G$  values (Table 4). The idea was also to check whether the prediction of the pathogenicity of these variants fit with the clinical and electrophysiological data. The DDMut server indicated that p.(His205Gln)/p.(Ser409Leu), p.(Leu377His), p.(Pro493Leu), and p(Gly587Asp) variants induced destabilizing effects on HCN2 structures at both depolarized and hyperpolarized states. Interestingly, high destabilizing effects were determined for

p.(His205Gln)/p.(Ser409Leu), p.(Pro493Leu), and p.(Gly587Asp) variants and p.(Gly460Asp) variant has a very weak stabilizing effect. In contrast, p.(Arg324His), p.(Arg324Cys), p.(Ala363Val), p.(Asn369Ser) and p.(Met374Leu) variants show positive  $\Delta\Delta G$  values, indicating stabilizing effects on HCN2 structure (Table 4). Thus, we carefully examined the 3D structure of each HCN2 variant 3D model structure to identify possible structural damage induced by these variants.

The p.(Arg324His) and p.(Arg324Cys) variants concern the second positively charged residue of S4. In the depolarized state (or close conformation), Arg324 side chain is oriented towards the extracellular compartment and thus freely exposes its positive charge. Interestingly, during HCN2 opening, S4 rotates counterclockwise, burying the Arg324 side chain in a hydrophobic pocket which is composed by Ile233, Leu323, Tyr317, Leu323, Phe328, Met391 and Leu391 (Fig. 6A). The ASA values of Arg324 dropped from  $139.27 \text{ \AA}^2$  (RSA = 64%) to  $24.07 \text{ \AA}^2$  (RSA = 14.12%) between depolarized state and hyperpolarized state (Table 4). In p.(Arg324His) variant, the shorter side chain of His, at position 324, fitted better in this hydrophobic pocket in the hyperpolarized state (ASA =  $14.12 \text{ \AA}^2$ , RSA = 7%) and could be stabilized by  $\pi$ - interaction with Tyr317 and Phe328 (Fig. 7B, lower left panel). In p.(Arg324Cys), Cys, which is more hydrophobic than Arg and His, can also be more stabilized in the hydrophobic pocket than Arg (ASA =  $9.44 \text{ \AA}^2$ , RSA = 7%) (Fig. 6B, lower right panel).

The next variant, p.(Ala363Val) involves important changes in the N-terminus of  $\alpha$ -helix S5, which impacted hydrophobic interaction with two leucines (Leu465 and Leu 469) in  $\alpha$ -helix S6, which are in the nearest-neighbour of Ala363 (Fig. 6C). During channel opening, the side chain of Ala363 is closer to these residues. At this position, Val, which is bulkier and more hydrophobic, could form stronger hydrophobic interaction with Leu465 and Leu469 (Fig. 6C, right panels). These two leucines are even closer to Ala in the

hyperpolarized state (Fig. 6C, lower right panel). This could affect the stability of the hyperpolarized state of HCN2 and might accelerate its activation kinetics, in agreement with the positive value of  $\Delta\Delta G$  identified with DDMut (Supplementary Table 5). In addition, the p.(Aal363Val) variant induced a decrease of molecule flexibility (with  $\Delta\Delta SVib ENCoM$  values of -0.626 and -0.287 kcal.mol<sup>-1</sup>.K<sup>-1</sup>, respectively) at both depolarized and hyperpolarized states.

In the depolarized state of HCN2, the side chain of Met374 is in sandwich between Phe458 and Met425 of  $\alpha$ -helix S6, while in the hyperpolarized, it goes between Phe458 and the backbone of Cys454 (Fig. 6D, left panels). In p.(Met374Leu) structure, a Leu at position 374 exhibits a different orientation with stronger interaction with Met425. This might strongly impact these interactions and involves important changes in the interface between  $\alpha$ -helix S5 and S6, and consecutively HCN2 opening (Fig. 6D, right panels). This is supported by the increase of  $\Delta\Delta G$  values, and reorganization of the S4-S5 segment during channel opening already reported.<sup>42</sup> Moreover, the p.(Met374Leu) variant induced an increase of flexibility of the molecule at the depolarized state ( $\Delta\Delta SVib ENCoM = -0.309$  kcal.mol<sup>-1</sup>.K<sup>-1</sup>), while this mutation led to increased rigidity at the hyperpolarized state ( $\Delta\Delta SVib ENCoM = 0.063$  kcal.mol<sup>-1</sup>.K<sup>-1</sup>).

In the depolarized state of wt-HCN2, Leu377 makes strong hydrophobic interactions with Val450 and Cys454, at the interface between S5 and S6 (Fig. 6D, upper left panel). Apparently, these interactions are absent in the hyperpolarized state, suggesting that the opening breaks them (Fig. 6D, lower left panel). In the depolarized state of p.(Leu377His) variant, the side chain of His exhibits a different orientation than Leu and could strongly interact with Asp381 through a salt bridge (Fig. 6D, upper right panel). In addition, with His at position 377, all hydrophobic interactions at the S5 and S6 interface are lost. Thus, the

structural modifications induced by a His at this position might explain the LOF of HCN2 and account for the large leak currents associated with this construct (Fig. 4A).

In the C-linker of HCN2, the p.(Pro493Leu) and p.(Glu587Asp) variants modify residues which are buried and important for the structure and dynamics of HCN2. Since Pro493 stabilizes the kink between the A' and B' anti-parallel helices by interacting with Phe533 of a neighbour subunit, the Pro493Leu mutation should thus strongly destabilize the channel structure (Fig. 6E). Gly587 is located at a central turn of the CNBD  $\beta$  core, in the vicinity of Lys187 of a neighbour subunit (Fig. 6F). Its substitution by an aspartic acid should lead to a salt bridge between the CNBD and the channel N-terminus. In addition, the Phi/Psi angles are outlier with G587D mutation.

We also performed a structural analysis of p.(His205Gln)/p.(Ser409Leu), p.(Asn369Ser) and p.(Gly460Asp) variants and highlighted their structural differences with wt-HCN2. The trans variant p.(His205Gln)/p.(Ser409Leu) variant showed profound structural changes (neutralisation of a buried charge, disruption of salt bridge between His205 and Glu192 in helix HCNC and loss of aromatic interaction between H205 and F183 of helix HCNC and Y207 (Supplementary Fig. 4A). Thus, we assumed that the trans variant p.(His205Gln)/p.(Asn369Ser) could have a deleterious impact on HCN2 function. The p.(Asn369Ser) variant leads to the loss of a hydrogen bond with Glu351 in S4 (Supplementary Fig. 5A). Finally, the p.(Gly460Asp) variant impacts the interface between S6 from two adjacent subunits, leading to clash with Ala462, Thr463 and Ile466 (Supplementary Fig. 6).

## **Phenotypic differences between individuals with GOF and LOF variants**

In individuals carrying a GOF variant (n = 18, including the 3 individuals from Family 2 and 15 individuals in the literature), seizures were present in 16/18 (89%) (FS only in

8/16, epilepsy in 8/16) with median age of onset of 5 years, but intellectual disability was present in only 1/18 individuals (5.5%) (Table 2). In individuals carrying LOF variants (n = 12, being individuals 6, 7, 9, 10, 11, 12, 16, 17, 18, 19 from this cohort and two individuals from literature), epilepsy was present in 8/12 (67%) with median age of onset of 7.5 months. ID was present in 11/12 (92%) individuals (not stated in one individual), being of moderate severity in two individuals with monoallelic LOF and severe-profound in three individuals with biallelic LOF. Of the 12 individuals whose variants have not been studied functionally, the six with biallelic variants all had severe DD/ID (Table 2).

## Discussion

In this study, by describing twenty-one additional individuals with deleterious *HCN2* variants, we expand the phenotype of *HCN2*-related disorders, from mild epilepsies with normal cognition, to phenotypes, including ID with or without epilepsy, and individuals with DEE. We reported twelve novel *HCN2* variants and highlight by combining electrophysiological and trafficking data with 3D-modelling that these variants can cause either GOF (monoallelic variants) or partial LOF (monoallelic variants) or complete LOF (biallelic variants). Taken together, we provide preliminary evidence of phenotype-genotype correlation: specifically, that LOF variants may be associated with more severe ID and, where epilepsy is present, earlier age of seizure onset.

We provide comprehensive electrophysiological and structural analysis to demonstrate that some variants lead to loss of HCN2 channel function. Our electrophysiological data clearly demonstrated that p.(Ala363Val) and p.(Met374Leu) variants strongly impair HCN2 operation, but still exhibit the main features of an hyperpolarized-activated ion channel. Indeed, both the p.(Ala363Val) and p.(Met374Leu) variants cause a strong decrease of current densities and a visible alteration of current kinetics. The negative shift of activation properties of both variants also indicates an impairment of the voltage-dependency. Thus, we attribute these alterations to a partial LOF of HCN2. This assumption is reinforced by the examination of our 3D-model, suggesting modification in the interactions of Ala363 and Met374 with Leu465 and Phe468 in S5, respectively. Altogether, we hypothesize that p.(Ala363Val) and p.(Met374Leu) variants alter the interactions between the S4, containing the voltage sensor and S5. The detrimental effects of mutations in the S4-S5 regions of tetrameric  $K_V$  and related HCN channels, is increasingly well documented with reports of cation leakage and gating blocks.<sup>23,43,44</sup> Interestingly, the p.(Met305Leu) HCN1 variant, which is an homologous variant to the p.(Met374Leu) variant has been associated with DEE.<sup>44</sup> While the p.(Met 374Leu) HCN2 variant shows similar current kinetics to the p.(Met305Leu) HCN1 variant, the instantaneous tail currents elicited by both variants shift in opposite direction.<sup>22</sup> This could be explained by biophysical specificities of HCN1 versus HCN2. In conclusion, p.(Ala363Val) and p.(Met374Leu) variants likely cause a partial LOF of HCN2, which could impair neuronal excitability.

In contrast, p.(Leu377His), p.(Pro493Leu) and p.(Gly587Asp) variants produce HCN2 proteins which are electrophysiologically silent in *Xenopus* oocytes. The p.(Leu377His) would impair the opening of HCN2 through the loss of the interaction with Gly450 in S6. The p.(Pro493Leu) variant could strongly destabilize the channel structure through the alteration of the interaction of the kink between the A' and B' anti-parallel helices of a

neighbour subunit. The p.(Gly587Asp) variant located in the CNBD, would not influence cyclic-nucleotide binding, but the aspartate could form a salt bridge with Lys187 in the N-terminal HCN domain, disrupting channel gating.<sup>45</sup> In addition, these three variants could not be detected at the plasma membrane, indicating that p.(Leu377His), p.(Pro493Leu) and p.(Gly587Asp) variants impair HCN2 membrane trafficking. To date, only two variants that alter membrane trafficking in HCN channels family have been reported, one in HCN4 p.(Pro257Ser) and one in HCN2 p.(Gly460Asp), associated with early-onset atrial fibrillation and DEE, respectively.<sup>28,46</sup> We assumed that the trafficking-impairment p.(Leu377His) variant might be the consequence of the misfolding of HCN2, while p.(Pro493Leu) and p.(Gly587Asp) variants could affect the interaction with trafficking regulating proteins, such as TRIP8b.<sup>35</sup> Altogether, p.(Leu377His), p.(Pro493Leu) and p.(Gly587Asp) variants are leading to complete LOF by impairing membrane trafficking.

Our study brings novel evidence to clearly establish LOF as a mechanism of HCN2-related disease, building on two previous case reports. As recently suggested by DiFrancesco, who reported that the p.(Gly460Asp) results in LOF, we believe that the pathogenicity of monoallelic LOF HCN2 variants is due to a dominant negative effect rather than haploinsufficiency, as evidenced by three observations.<sup>28</sup> Firstly, in our cohort (seven cases from four families) and the literature (one case), the heterozygous parents of a child with a homozygous biallelic variant were all unaffected. Secondly, disease-causing monoallelic truncating HCN2 variants have not been reported to date; similarly, truncating pathogenic variants have not been reported in *HCN1* or *HCN4*. Thirdly, data from the gnomAD database includes twelve truncating *HCN2* variants in healthy individuals, and a pLI score of 0.17 indicating a low probability that *HCN2* could be intolerant to loss of function.

We also provide data to advance understanding of GOF *HCN2* variants. The p.(Arg324His) variant led to an increase of HCN2 ion channel function as the result of an increase of



conductance and faster activation kinetics compared to wt-HCN2, while voltage-dependent activation properties are unchanged. In addition, the 3D-model did not reveal any modification at the molecular level in the depolarized state. However, in the hyperpolarized state, the side chain of the residue at position 324 falls into a hydrophobic pocket, which constitutes a more stabilizing environment for histidine and cysteine than for the arginine. The p.(Arg324His) variant could generate a lower electrostatic repulsion of cations at the extracellular side of the channel, which favors cations to flow through HCN2. Further molecular dynamic analysis will be required to better understand the impact of these mutations. Thus, the GOF caused by p.(Arg324His) variant results from an important increase of HCN2 conductance as reported for the p.(Pro719-Pro721del) variant, but also from faster activation kinetics, not seen for the p.(Pro719-Pro721del) variant (Table 1).<sup>24</sup> Two other monoallelic variants of *HCN2* (p.(Val246Met) and p.(Ser635Trp)) with GOF have been already described, while these variants exhibit unchanged conductance, they give faster currents and activation at less negative potential than wt-HCN2.<sup>27</sup> Overall, these findings highlight that, similar to other ion channelopathies, GOF can arise from disruption of a number of different aspects of HCN2 channel function.

With this cohort, we confirm that pathogenic *HCN2* variants can be associated with more severe phenotypes than previously reported.<sup>24-27</sup> To date, only six variants – p.(Pro719-Pro721del), p.(Val246Met), p.(Ser632Trp), p.(Glu515Lys), p.(Ser126Leu) and p.(Gly460Asp) – of *HCN2* have been reported in 18 individuals with relatively mild forms of epilepsy including GGE and GEFS+ and most of them had no ID.<sup>24-28</sup> In contrast, seventeen out of the twenty-one individuals reported here have mild to profound ID and only ten have a history of seizures. The epilepsy phenotypes in the individuals in our cohort are variable, and most do not have features consistent with a named epilepsy syndrome. Abnormal tone, movement disorders, particularly dystonia and stereotypies, and nystagmus

are common symptoms, being present in 76%, 48% and 38% of individuals respectively; all these neurological findings broaden the phenotypic spectrum associated with *HCN2*. Five individuals have abnormal brain imaging, showing similar patterns of bilateral periventricular or subcortical white matter hyperintensities; this pattern is not reported in the remaining individuals. We did not identify other common symptoms in the group, although acknowledge that some may have been under-recognized or under-reported.

Similar to *HCN1*, our data and the literature allowed us to highlight limited genotype-phenotype correlation for *HCN2*-related conditions (Table 1). Seizures were a common but not universal feature in those with either GOF or LOF variants, being present in 89% (16/18) and 67% (8/12) respectively. However, only 44% (8/18) individuals with GOF variants had epilepsy, the remaining individuals having FS only. Additionally, the age of epilepsy onset was earlier in those with LOF variants (median 7.5 months) compared with GOF variants (median 5 years). DD/ID was present more frequently and was more severe in those with LOF variants (present in 11/12 individuals (92%), range moderate-severe) than with GOF variants (present in 1/18 individuals (6%), range normal-mild). We note that features other than the *HCN2* variant likely contribute to disease severity: we saw intrafamilial variability in severity for family 2 with the monoallelic p.(Arg324His) variant and for families 7, 11 and 14 carrying the homozygous p.(Leu377His), p.(Pro493Leu) and p.(Met647HisfsTer31) variants, respectively. Additionally, we noted interindividual variability for the two individuals carrying the monoallelic p.(Ala363Val) variant in terms of ID severity and presence of epilepsy; and the three individuals carrying the inframe p.Glu478del variant, with variability in severity of visual impairment and movement disorder.

Taken together, our data indicate that the related HCN2 phenotype, ranging from febrile seizures or mild epilepsy without ID, to severe forms of epilepsy with ID and ID without epilepsy, is very similar to that caused by HCN1 variants.<sup>23</sup> Thus, one characteristic shared by both isoforms *HCN1* and *HCN2* is the wide phenotypic spectrum caused by channel disruption. A relevant difference between *HCN1* and *HCN2* is the absence of reported biallelic pathogenic variants in *HCN1*, while biallelic inheritance is frequent in our HCN2 cohort. Interestingly, monoallelic and biallelic pathogenic variants have also been described for genes encoding other ion channels, such as *SCN1B* and *CACNA1D*, both of which have been implicated in severe forms of epilepsy.<sup>47,48</sup>

We acknowledge limitations of our work, including that we did not perform functional studies on all the identified *HCN2* variants, and therefore cannot confidently determine whether they result in GOF or LOF, although we would expect LOF for the biallelic variants. However, the structural analyses of the monoallelic variants - p.(Arg324Cys), p.(Asn369Ser) and p.(Glu478del) - the biallelic p.(Met647HisfsTer31) variant and the two heterozygous compound variants - p.(His205Gln) and p.(Ser409Leu) - suggest significant structural impacts and consequently HCN2 channel dysfunctions (Supp. Fig. 3). Furthermore, there remain some unanswered questions about the impact of each variant on channel function. As performed elsewhere, molecular dynamic simulation studies of the effect of these variants on HCN2 channel 3D-structure would provide additional information on the alteration of gating mechanisms.<sup>23,49</sup> At a neuronal circuit and whole brain level, the implications of HCN2 channel dysfunction are yet to be elucidated. The use of stem cell and organoid models, and generation of transgenic mice, will advance understanding of disease mechanisms, and provide models upon which to develop targeted therapies, as done recently for *HCN1*.<sup>50</sup>

In conclusion, our findings highlight the association of mono (n = 7) and bi-allelic (n = 6) *HCN2* variants with ID with or without epilepsy. To date, the p.(Leu377His), p.(Pro493Leu) and p.(Gly587Asp) variants represent the first cases of bi-allelic *HCN2* variants causing a complete LOF. Finally, these data are strongly supported by electrophysiological and structural results disclosing that both GOF and LOF variants are responsible for *HCN2*-related neurodevelopmental disorders.

## **Acknowledgements**

We are very grateful to the patients and their family for their participation in this study. We would also like to thank the Groupama Foundation “Vaincre les maladies rares” for its financial support.

## **Funding**

This work was supported by a grant from the Groupama Foundation “Vaincre les maladies rares”. For individual 1, sequencing and analysis were provided by the Broad Institute of MIT and Harvard Center for Mendelian Genomics (Broad CMG) and were funded by the National Human Genome Research Institute grants UM1 HG008900 (with additional support from the National Eye Institute, and the National Heart, Lung and Blood Institute), U01HG011755, and R01 HG009141, and in part by grant number 2020-224274 from the Chan Zuckerberg Initiative DAF, an advised fund of Silicon Valley Community Foundation. For individual 8, SS received funding by the Dietmar Hopp Stiftung [1DH1813319]. Dr

Howell was supported by the Melbourne Children's Clinician Scientist Fellowship scheme, and grants from the National Health and Medical Research Council and the Medical Research Futures Fund. Dr Howell has received project funding (for unrelated work) from Praxis Precision Medicines, RogCon, Inc, and UCB Australia. The Murdoch Children's Research Institute is supported by the Victorian State Government Operational Infrastructure Program.

## **Competing interests**

The authors report no competing interests.

## **Supplementary material**

Supplementary material is available.

## **Appendix 1**

This section is included if the article contains an appendix, for example, to list consortium collaborators who must be indexed online.

## **References**

1. Reid CA, Berkovic SF, Petrou S. Mechanisms of human inherited epilepsies. *Progress in Neurobiology*. 2009;87(1):41-57. doi:10.1016/j.pneurobio.2008.09.016
2. Avanzini G, Franceschetti S, Mantegazza M. Epileptogenic Channelopathies: Experimental Models of Human Pathologies. *Epilepsia*. 2007;48(s2):51-64. doi:10.1111/j.1528-1167.2007.01067.x

3. Kessi M, Chen B, Peng J, Yan F, Yang L, Yin F. Calcium channelopathies and intellectual disability: a systematic review. *Orphanet J Rare Dis.* 2021;16:219. doi:10.1186/s13023-021-01850-0
4. Biel M, Wahl-Schott C, Michalakis S, Zong X. Hyperpolarization-Activated Cation Channels: From Genes to Function. *Physiological Reviews.* 2009;89(3):847-885. doi:10.1152/physrev.00029.2008
5. Poolos NP. Hyperpolarization-Activated Cyclic Nucleotide-Gated (HCN) Ion Channelopathy in Epilepsy. In: Noebels J, Avoli M, Rogawski M, Olsen R, Delgado-Escueta A, eds. *Jasper's Basic Mechanisms of the Epilepsies.* Oxford University Press; 2012:85-96. doi:10.1093/med/9780199746545.003.0007
6. Huang Z, Walker MC, Shah MM. Loss of Dendritic HCN1 Subunits Enhances Cortical Excitability and Epileptogenesis. *Journal of Neuroscience.* 2009;29(35):10979-10988. doi:10.1523/JNEUROSCI.1531-09.2009
7. Noam Y, Bernard C, Baram TZ. Towards an integrated view of HCN channel role in epilepsy. *Curr Opin Neurobiol.* 2011;21(6):873-879. doi:10.1016/j.conb.2011.06.013
8. Kessi M, Peng J, Duan H, et al. The Contribution of HCN Channelopathies in Different Epileptic Syndromes, Mechanisms, Modulators, and Potential Treatment Targets: A Systematic Review. *Front Mol Neurosci.* 2022;15:807202. doi:10.3389/fnmol.2022.807202
9. Chen J. Voltage Sensing and Activation Gating of HCN Pacemaker Channels. *Trends in Cardiovascular Medicine.* 2002;12(1):42-45. doi:10.1016/S1050-1738(01)00141-4
10. Thon S, Schmauder R, Benndorf K. Elementary Functional Properties of Single HCN2 Channels. *Biophys J.* 2013;105(7):1581-1589. doi:10.1016/j.bpj.2013.08.027
11. Lee CH, MacKinnon R. Structures of the human HCN1 hyperpolarization-activated channel. *Cell.* 2017;168(1-2):111-120.e11. doi:10.1016/j.cell.2016.12.023
12. Moroni A, Barbuti A, Altomare C, et al. Kinetic and ionic properties of the human HCN2 pacemaker channel. *Pflugers Arch - Eur J Physiol.* 2000;439(5):618-626. doi:10.1007/s004249900225
13. Benarroch EE. HCN channels: Function and clinical implications. *Neurology.* 2013;80(3):304-310. doi:10.1212/WNL.0b013e31827dec42
14. Difrancesco D. Serious workings of the funny current. *Progress in Biophysics and Molecular Biology.* 2006;90(1-3):13-25. doi:10.1016/j.pbiomolbio.2005.05.001
15. Schulze-Bahr E, Neu A, Friederich P, et al. Pacemaker channel dysfunction in a patient with sinus node disease. *J Clin Invest.* 2003;111(10):1537-1545. doi:10.1172/JCI200316387
16. Wainger BJ, DeGennaro M, Santoro B, Siegelbaum SA, Tibbs GR. Molecular mechanism of cAMP modulation of HCN pacemaker channels. *Nature.* 2001;411(6839):805-810. doi:10.1038/35081088

17. Lewis AS, Chetkovich DM. HCN channels in behavior and neurological disease: too hyper, or not active enough? *Mol Cell Neurosci.* 2011;46(2):357-367. doi:10.1016/j.mcn.2010.11.007
18. Hammelmann V, Stieglitz MS, Hülle H, et al. Abolishing cAMP sensitivity in HCN2 pacemaker channels induces generalized seizures. *JCI Insight.* 4(9):e126418. doi:10.1172/jci.insight.126418
19. Ludwig A. Absence epilepsy and sinus dysrhythmia in mice lacking the pacemaker channel HCN2. *The EMBO Journal.* 2003;22(2):216-224. doi:10.1093/emboj/cdg032
20. Chung WK, Shin M, Jaramillo TC, et al. Absence epilepsy in apathetic, a spontaneous mutant mouse lacking the h channel subunit, HCN2. *Neurobiol Dis.* 2009;33(3):499-508. doi:10.1016/j.nbd.2008.12.004
21. EuroEPINOMICS RES Consortium, Nava C, Dalle C, et al. De novo mutations in HCN1 cause early infantile epileptic encephalopathy. *Nat Genet.* 2014;46(6):640-645. doi:10.1038/ng.2952
22. Specchio N, Curatolo P. Developmental and epileptic encephalopathies: what we do and do not know. *Brain.* 2021;144(1):32-43. doi:10.1093/brain/awaa371
23. Marini C, Porro A, Rastetter A, et al. *HCN1* mutation spectrum: from neonatal epileptic encephalopathy to benign generalized epilepsy and beyond. *Brain.* 2018;141(11):3160-3178. doi:10.1093/brain/awy263
24. Dibbens LM, Reid CA, Hodgson B, et al. Augmented currents of an HCN2 variant in patients with febrile seizure syndromes. *Annals of Neurology.* 2010;67(4):542-546. doi:https://doi.org/10.1002/ana.21909
25. DiFrancesco JC, Barbuti A, Milanesi R, et al. Recessive Loss-of-Function Mutation in the Pacemaker HCN2 Channel Causing Increased Neuronal Excitability in a Patient with Idiopathic Generalized Epilepsy. *Journal of Neuroscience.* 2011;31(48):17327-17337. doi:10.1523/JNEUROSCI.3727-11.2011
26. Nakamura Y, Shi X, Numata T, et al. Novel HCN2 Mutation Contributes to Febrile Seizures by Shifting the Channel's Kinetics in a Temperature-Dependent Manner. *PLoS One.* 2013;8(12):e80376. doi:10.1371/journal.pone.0080376
27. Li M, Maljevic S, Phillips AM, et al. Gain-of-function HCN2 variants in genetic epilepsy. *Human Mutation.* 2018;39(2):202-209. doi:https://doi.org/10.1002/humu.23357
28. DiFrancesco JC, Ragona F, Murano C, et al. A novel de novo HCN2 loss-of-function variant causing developmental and epileptic encephalopathy treated with a ketogenic diet. *Epilepsia.* n/a(n/a). doi:10.1111/epi.17777
29. Dibbens LM, Reid CA, Hodgson B, et al. Augmented currents of an HCN2 variant in patients with febrile seizure syndromes. *Ann Neurol.* 2010;67(4):542-546. doi:10.1002/ana.21909
30. Sobreira N, Schiettecatte F, Valle D, Hamosh A. GeneMatcher: A Matching Tool for Connecting Investigators with an Interest in the Same Gene. *Human Mutation.* 2015;36(10):928-930. doi:10.1002/humu.22844

31. Riney K, Bogacz A, Somerville E, et al. International League Against Epilepsy classification and definition of epilepsy syndromes with onset at a variable age: position statement by the ILAE Task Force on Nosology and Definitions. *Epilepsia*. 2022;63(6):1443-1474. doi:10.1111/epi.17240
32. Richards S, Aziz N, Bale S, et al. Standards and Guidelines for the Interpretation of Sequence Variants: A Joint Consensus Recommendation of the American College of Medical Genetics and Genomics and the Association for Molecular Pathology. *Genet Med*. 2015;17(5):405-424. doi:10.1038/gim.2015.30
33. Park J, Taly A, Bourreau J, et al. Partial Agonist Activity of Neonicotinoids on Rat Nicotinic Receptors: Consequences over Epinephrine Secretion and In Vivo Blood Pressure. *Int J Mol Sci*. 2021;22(10):5106. doi:10.3390/ijms22105106
34. Mattei C, Taly A, Soualah Z, et al. Involvement of the GABAA receptor  $\alpha$  subunit in the mode of action of etifoxine. *Pharmacological Research*. 2019;145:104250. doi:10.1016/j.phrs.2019.04.034
35. Santoro B, Wainger BJ, Siegelbaum SA. Regulation of HCN Channel Surface Expression by a Novel C-Terminal Protein-Protein Interaction. *J Neurosci*. 2004;24(47):10750-10762. doi:10.1523/JNEUROSCI.3300-04.2004
36. Sali A, Blundell TL. Comparative protein modelling by satisfaction of spatial restraints. *J Mol Biol*. 1993;234(3):779-815. doi:10.1006/jmbi.1993.1626
37. Saponaro A, Bauer D, Giese MH, et al. Gating movements and ion permeation in HCN4 pacemaker channels. *Molecular Cell*. 2021;81(14):2929-2943.e6. doi:10.1016/j.molcel.2021.05.033
38. Saponaro A, Thiel G, Moroni A. Structural and functional approaches to studying cAMP regulation of HCN channels. *Biochemical Society Transactions*. 2021;49(6):2573-2579. doi:10.1042/BST20210290
39. Zhou Y, Pan Q, Pires DEV, Rodrigues CHM, Ascher DB. DDMut: predicting effects of mutations on protein stability using deep learning. *Nucleic Acids Research*. 2023;51(W1):W122-W128. doi:10.1093/nar/gkad472
40. Rodrigues CH, Pires DE, Ascher DB. DynaMut: predicting the impact of mutations on protein conformation, flexibility and stability. *Nucleic Acids Research*. 2018;46(W1):W350-W355. doi:10.1093/nar/gky300
41. Mistrík P, Pfeifer A, Biel M. The enhancement of HCN channel instantaneous current facilitated by slow deactivation is regulated by intracellular chloride concentration. *Pflugers Arch - Eur J Physiol*. 2006;452(6):718-727. doi:10.1007/s00424-006-0095-0
42. Li M, Tonggu L, Tang L, Wang L. Effects of N-glycosylation on hyperpolarization-activated cyclic nucleotide-gated (HCN) channels. *Biochemical Journal*. 2015;466(1):77-84. doi:10.1042/BJ20140692
43. Hung A, Forster IC, McKenzie CE, et al. Biophysical analysis of an HCN1 epilepsy variant suggests a critical role for S5 helix Met-305 in voltage sensor to pore domain coupling. *Progress in Biophysics and Molecular Biology*. 2021;166:156-172. doi:10.1016/j.pbiomolbio.2021.07.005



44. Bleakley LE, McKenzie CE, Soh MS, et al. Cation leak underlies neuronal excitability in an HCN1 developmental and epileptic encephalopathy. *Brain*. 2021;144(7):2060-2073. doi:10.1093/brain/awab145
45. Porro A, Saponaro A, Gasparri F, et al. The HCN domain couples voltage gating and cAMP response in hyperpolarization-activated cyclic nucleotide-gated channels. *eLife*. 8:e49672. doi:10.7554/eLife.49672
46. Macri V, Mahida SN, Zhang ML, et al. A novel trafficking-defective HCN4 mutation is associated with early-onset atrial fibrillation. *Heart Rhythm*. 2014;11(6):1055-1062. doi:10.1016/j.hrthm.2014.03.002
47. Scala M, Efthymiou S, Sultan T, et al. Homozygous SCN1B variants causing early infantile epileptic encephalopathy 52 affect voltage-gated sodium channel function. *Epilepsia*. 2021;62(6):e82-e87. doi:10.1111/epi.16913
48. Wengert ER, Tronhjem CE, Wagnon JL, et al. Biallelic inherited SCN8A variants, a rare cause of SCN8A-related developmental and epileptic encephalopathy. *Epilepsia*. 2019;60(11):2277-2285. doi:10.1111/epi.16371
49. Hung A, Forster IC, McKenzie CE, et al. Biophysical analysis of an HCN1 epilepsy variant suggests a critical role for S5 helix Met-305 in voltage sensor to pore domain coupling. *Prog Biophys Mol Biol*. 2021;166:156-172. doi:10.1016/j.pbiomolbio.2021.07.005
50. Bleakley LE, Keenan RJ, Graven RD, et al. Altered EEG power spectrum, but not sleep-wake architecture, in HCN1 knockout mice. *Behavioural Brain Research*. 2023;437:114105. doi:10.1016/j.bbr.2022.114105

## Figure legends

**Figure 1 Pedigrees and *HCN2* pathogenic variants** (A) *HCN2* channel and pathogenic variants. Variants identified in the cohort are indicated by red stars, variants previously reported are indicated by black stars. Biallelic variants are underlined while monoallelic are not. Pink dotted line, green full line and green dotted line indicate HCN domain, C-linker, and CNBD, respectively. (B) Pedigrees of I1–21 and multi-species sequence alignment of the mutated *HCN2* channels. (a-i) Pedigree and multi-species sequence alignment of I1-21. Multi-species sequence alignment was performed using Clustal Omega {Uniprot entries: A0A8N7T6V3 (*Danio rerio*), A0A8V1AGR5 (*Gallus gallus*), O88703 (*Mus musculus*), Q9UL51 (*Homo sapiens*)}. Below the sequence alignment, a key denotes conserved amino acid (\*), conservative replacement (:) and non-conservative replacement (). When not mentioned, the individual's genotype is unknown.

**Figure 2 Electrophysiological characterization of wt-*HCN2* and the monoallelic variants, p.(Arg324His), p.(Ala363Val) and p.(Met374Leu).** (A) Examples of superimposed current traces, representing the current families, developed in response to hyperpolarized stimulations. From left to right, example of currents elicited by uninjected oocytes (NI), wt-*HCN2* channel (WT), wt/p.(Arg324His) (WT + R324H), wt/p.(Ala363Val) (WT + A363V) and, wt/p.(Met374Leu) (WT + M374L) channels, respectively. (B to D) From left to right, the I/V curves were built using current densities measured at the steady-state and instantaneous components. Current densities for the slow component were then deduced. For each variant, significance of difference with wt-*HCN2* was analysed with a two-way ANOVA test (corrected with Geisser-Greenhouse method), followed by a comparison test (two-stage step-up method of Benjamini, Kriger and Yekutieli). Data are

shown as mean  $\pm$  SEM. For clarity, no information indicates no significance. \*,  $P < 0.05$ ; \*\*,  $P < 0.01$ ; \*\*\*,  $P < 0.001$ ; \*\*\*\*,  $P < 0.0001$ .

**Figure 3 Activation kinetics and tail current analysis for wt-HCN2 and the monoallelic variants, p.(Arg324His), p.(Ala363Val) and p.(Met374Leu).** (A) Examples of traces showing the slow component of currents elicited by wt-HCN2 channel (WT), wt/p.(Arg324His) (WT + R324H), wt/p.(Ala363Val) (WT + A363V) and, wt/p.(Met374Leu) (WT + M374L) channels, respectively. (B) Current kinetics analysis. Current traces were well-fitted with a mono-exponential equation. Tau (ms) was plotted versus  $V_m$  (mV). For each variant, significance of difference with wt-HCN2 was analysed with a two-way ANOVA test (corrected with Geisser-Greenhouse method), followed by a comparison test (two-stage step-up method of Benjamini, Kriger and Yekutieli). (C) Representative tail current traces for wt-HCN2 channel (WT), wt/p.(Arg324His) (WT + R324H), wt/p.(Ala363Val) (WT + A363V) and, wt/p.(Met374Leu) (WT + M374L) channels, respectively. (D) Left panel shows normalized current amplitudes ( $I/I_{max}$ ) versus  $V_m$  were well-fitted with the Boltzmann equation, allowing the determination of the half-activation potentials ( $V_{1/2}$ ) and the slope factor  $k$ . Right panel shows the scatter plots show the comparison of the  $V_{1/2}$  (left) and slope factor (right) of the wt-HCN2, wt/p.(Ala363Val), wt/p.(Met374Leu) and wt/p.(Arg324His) mutant channels. A one-way ANOVA test ( $F = 53,15$ ,  $P < 0.0001$ ), followed by a Dunnett test, was performed and showed a significant difference between mutants and wt-HCN2, except between p.(Arg324His) and wt-HCN2 (p-value = 0.48). Data are shown as mean  $\pm$  SEM. ns, not significant; \*,  $P < 0.05$ ; \*\*,  $P < 0.01$ ; \*\*\*,  $P < 0.001$ ; \*\*\*\*,  $P < 0.0001$ .

**Figure 4 Characterization of p.(Leu377His), p.(Pro493Leu) and p.(Gly587Asp) HCN2 variants.** (A, C and E) Representative TEVC recordings from oocytes expressing HCN2 wild-type and two homozygous variants of HCN2, p.(Leu377His), p.(Pro493Leu) and p.(Gly587Asp). The data show current traces for voltage steps from -130 to -30 mV from a holding potential of -30 mV for 10 s. (B, D and F) Western blot of *Xenopus laevis* oocyte proteins. The panels show immunostaining with anti-HCN2 and anti- $\beta$ -actin antibodies. WT: oocytes injected with wt-HCN2 mRNA, NI: non-injected oocytes; L377H, P493L and G587D: oocytes injected with p.(Leu377His), p.(Pro493Leu) and p.(Gly587Asp) variants mRNAs, respectively. (G-J) Study of membrane trafficking of p.(Leu377His), p.(Pro493Leu) and p.(Gly587Asp) variants in HEK293 cells. The expression of EGFP-tagged p.(Leu377His) or p.(Pro493Leu) or p.(Gly587Asp) HCN2 variants was evaluated by confocal microscopy. The cells were stained with the CellMask orange membrane stain and DAPI nuclear stain. EGFP-tagged wt-HCN2 (G, left panel) shows a strong EGFP signal at the plasma membrane, while the trafficking-defected HCN2 $\Delta_{C-X}$  (Thr553Ter) shows cytosolic staining (G, right panel), as seen for p.(Leu377His), p.(Pro493Leu) and p.(Gly587Asp) variants (H-J). Examples of images obtained from magnification of 63x are shown (G and H-J, left panels). Examples of overview with magnification from 20x are also shown (H-J, left panels).

**Figure 5 Mutation mapping onto 3-dimensional homology models of HCN2 in depolarised and hyperpolarised states.** Models of HCN2 in depolarized (left panels) and hyperpolarized states (right panels) are shown (upper panels: profile views. lower panels: top views). Proteins are drawn in ribbon representation with a different color code for each subunit. For clarity, the locations of mutated amino acids are represented as spheres in only

one subunit (in cyan), while the other subunits are shown in semi-transparent representations. The approximate position of HCN2 within the membrane is visualized with the gray rectangle.

**Figure 6 Structural analysis of p.(Arg324His), p.(Ala363Val), p.(M374Leu), p.(Leu377His), p.(Pro493Leu) and p.(Gly587Asp) HCN2 pathogenic variants.** For clarity, zoom in of profile views were chosen for each mutation, except for p.(Arg324His) variant. **(A)** Top view of S1-S4 helices of wt-HCN2 and p.(Arg324His) HCN2 variant in the depolarized and hyperpolarized states. The side chain of residue at 324 is towards the solvent in the depolarized state of HCN2 (left panel), but after opening it remains trapped in a hydrophobic pocket formed by I233, L323, Y317, F328, M390 and L391. **(B, C and D)** Profile views of S5-S6 interfaces showing the residues A363 **(B)**, M374 **(C)** and L377 **(D)**. **(E and F)** The two last mutations are located in the intracellular region of HCN2 structure at the interfaces between two subunits (Chains B and C). The p.(Pro493Leu) variant **(E)** might destabilize the bend between helices A' and B' and also the N-terminal of helice B'. The p.(Gly587Asp) variant could change the curvature of the loop between two  $\beta$ -sheets within the CNBD **(F)**. The proteins are drawn in ribbon representation. and their closest-neighbour contacts with residues of S6. The distances are indicated in Å.

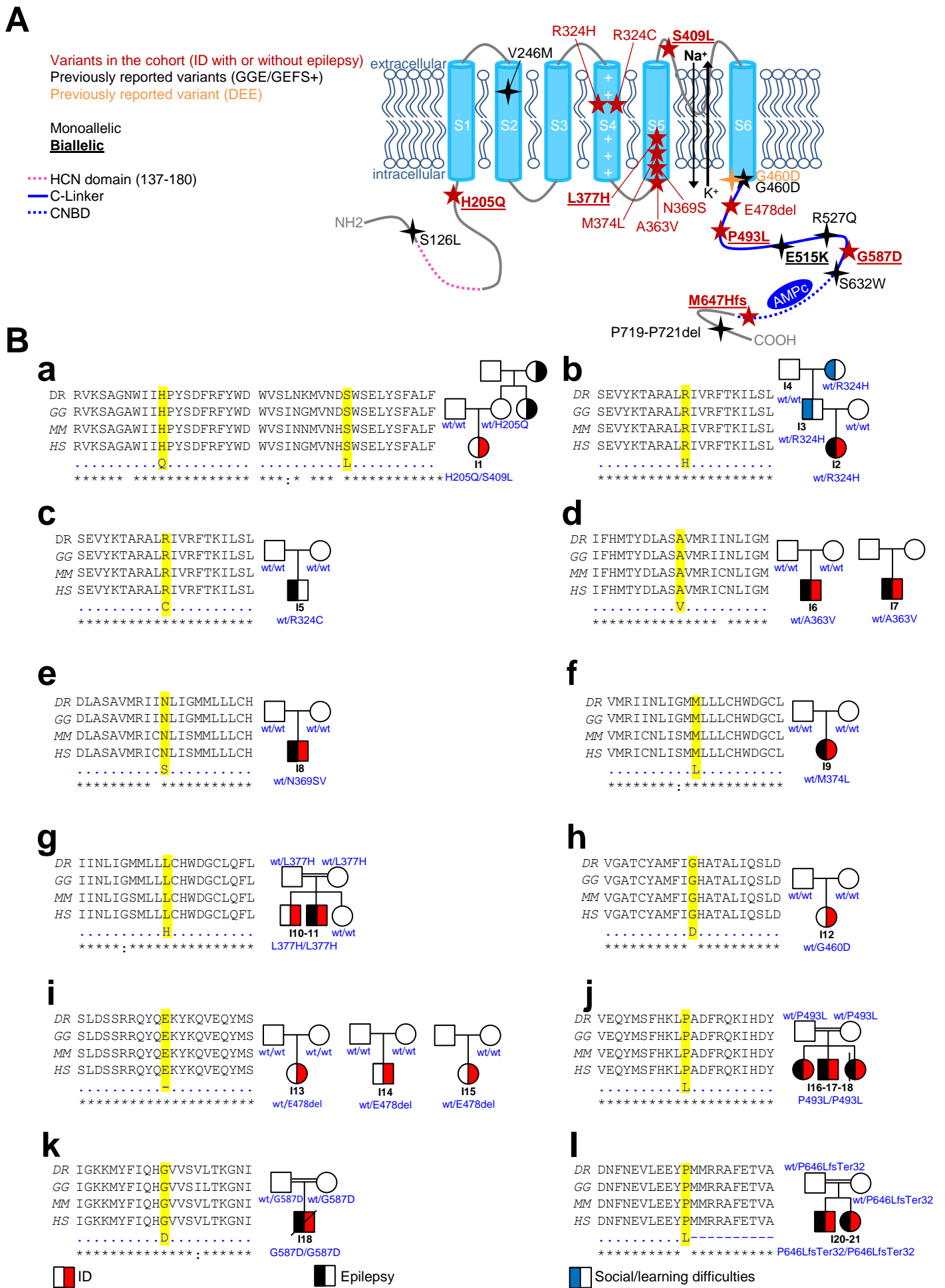


**Figure 1 Pedigrees and HCN2 pathogenic variants (A)** Pathogenic variants of HCN2. Red stars indicate HCN2 variants identified in this work, and black stars indicate those previously reported. Biallelic variants are underlined while monoallelic are not. **(B)** Pedigrees of I1–21 and multi-species sequence alignment of HCN2 variants (a–i). Sequence alignment was performed using Clustal Omega {Uniprot entries: A0A8N7T6V3 (*Danio rerio*), A0A8V1AGR5 (*Gallus gallus*), O88703 (*Mus musculus*), Q9UL51 (*Homo sapiens*)}. (\*), conserved amino-acid residue; (:), conservative replacement; ( ), non-conservative replacement. When not mentioned, the individual’s genotype is unknown.

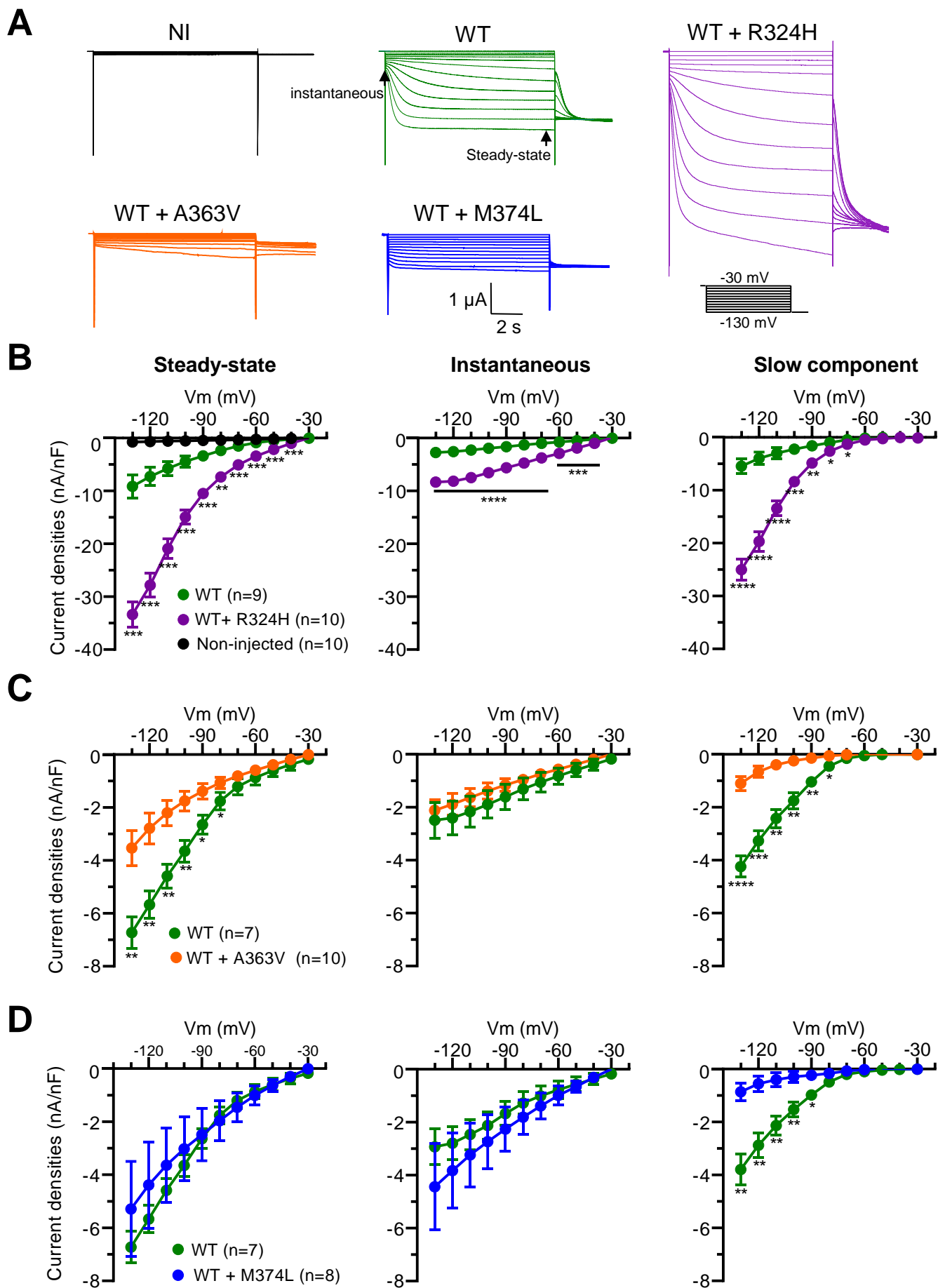


**Figure 2 Electrophysiological characterization of the monoallelic variants, p.(Arg324His), p.(Ala363Val) and p.(Met374Leu).** (A) Examples of superimposed current traces, developed in response to hyperpolarized stimulations. From left to right, example of currents elicited by uninjected oocytes (NI), wt-HCN2 channel (WT), wt/p.(Arg324His) (WT + R324H), wt/p.(Ala363Val) (WT + A363V) and, wt/p.(Met374Leu) (WT + M374L) channels, respectively. (B to D) From left to right, the I/V curves were built using current densities measured at the steady-state and instantaneous components. Current densities for the slow component were then deduced. For each variant, significance of difference with wt-HCN2 was analysed with a two-way ANOVA test (corrected with Geisser-Greenhouse method), followed by a comparison test (two-stage step-up method of Benjamini, Kriger and Yekutieli). Data are shown as mean  $\pm$  SEM. For clarity, no information indicates no significance. \*,  $P < 0.05$ ; \*\*,  $P < 0.01$ ; \*\*\*,  $P < 0.001$ ; \*\*\*\*,  $P < 0.0001$ .

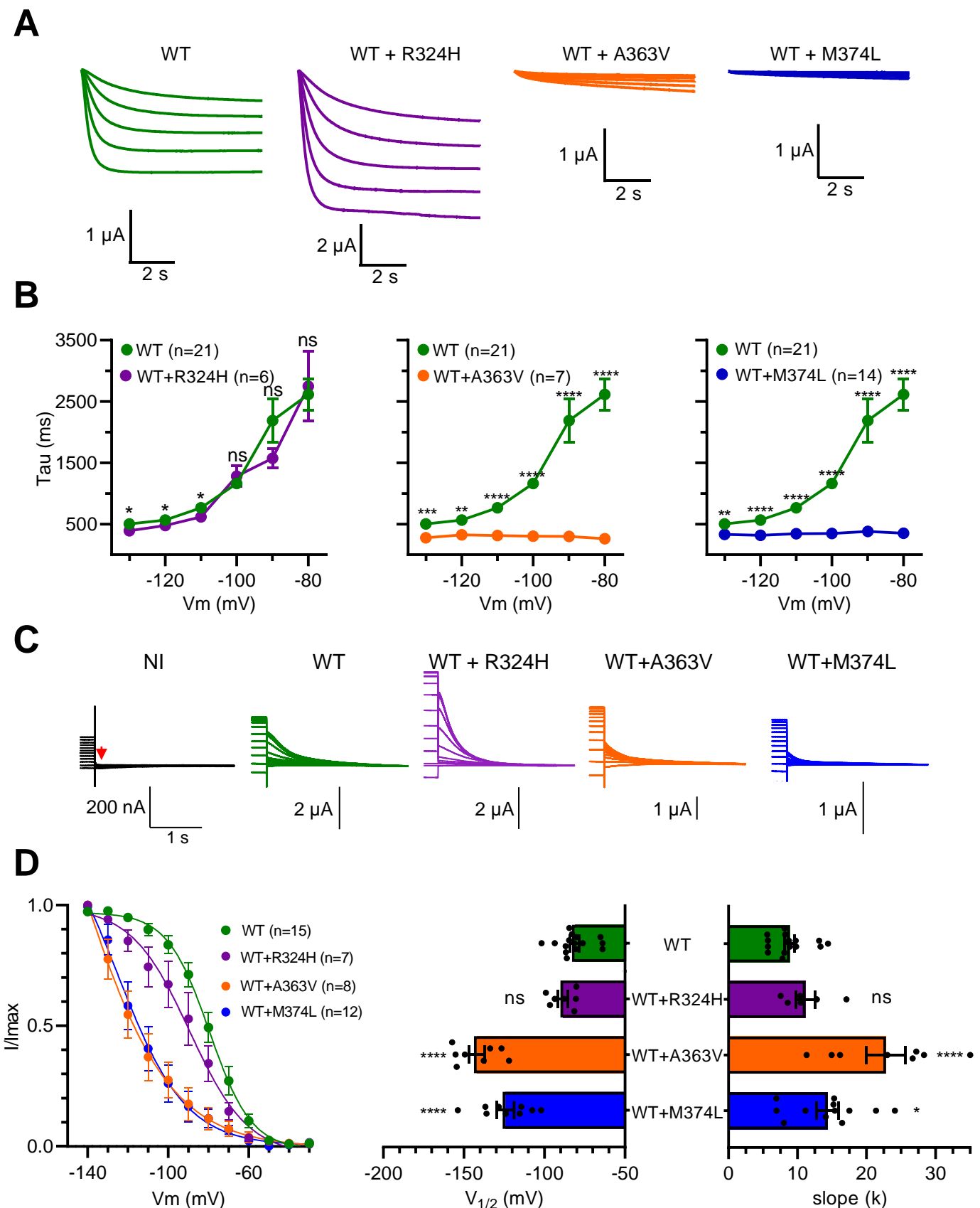


**Figure 3 Activation kinetics and tail current analysis for the monoallelic variants, p.(Arg324His), p.(Ala363Val) and p.(Met374Leu).** (A) Examples of traces showing the slow component of currents elicited by wt-HCN2 channel (WT), wt/p.(Arg324His) (WT + R324H), wt/p.(Ala363Val) (WT + A363V) and, wt/p.(Met374Leu) (WT + M374L) channels, respectively. (B) Current kinetics analysis. Current traces were well-fitted with a mono-exponential equation. Tau (ms) was plotted versus Vm (mV). For each variant, significance of difference with wt-HCN2 was analysed with a two-way ANOVA test (corrected with Geisser-Greenhouse method), followed by a comparison test (two-stage step-up method of Benjamini, Kriger and Yekutieli). (C) Representative tail current traces for wt-HCN2 channel (WT), wt/p.(Arg324His) (WT + R324H), wt/p.(Ala363Val) (WT + A363V) and, wt/p.(Met374Leu) (WT + M374L) channels, respectively. (D) Left panel shows normalized current amplitudes (I/Imax) versus Vm were well-fitted with the Boltzmann equation, allowing the determination of the half-activation potentials ( $V_{1/2}$ ) and the slope factor k. Right panel shows the scatter plots show the comparison of the  $V_{1/2}$  (left) and slope factor (right) of the wt-HCN2, wt/p.(Ala363Val), wt/p.(Met374Leu) and wt/p.(Arg324His) mutant channels. A one-way ANOVA test ( $F = 53,15$ ,  $P < 0.0001$ ), followed by a Dunnett test, was performed and showed a significant difference between mutants and wt-HCN2, except between p.(Arg324His) and wt-HCN2 ( $P = 0.48$ ). Data are mean  $\pm$  SEM. ns, not significant; \*,  $P < 0.05$ ; \*\*,  $P < 0.01$ ; \*\*\*,  $P < 0.001$ ; \*\*\*\*,  $P < 0.0001$ .



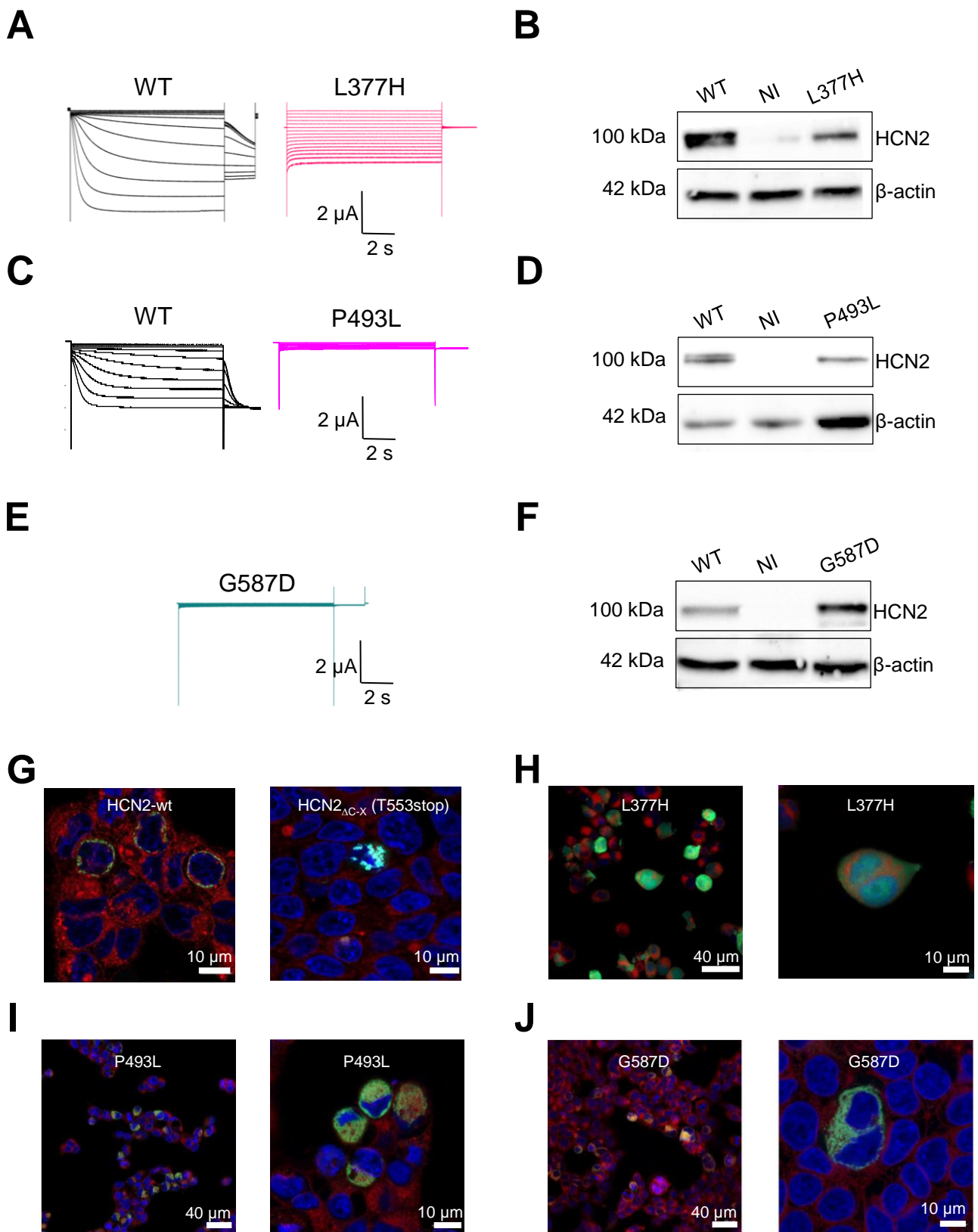


**Figure 4 Characterization of p.(Leu377His), p.(Pro493Leu) and p.(Gly587Asp) HCN2 variants.** (A, C and E) Representative TEVC recordings from oocytes expressing HCN2 wild-type and two homozygous variants of HCN2, p.(Leu377His), p.(Pro493Leu) and p.(Gly587Asp). The data show current traces for voltage steps from -130 to -30 mV from a holding potential of -30 mV for 10 s. (B, D and F) Western blot of *Xenopus laevis* oocyte proteins. The panels show immunostaining with anti-HCN2 and anti- $\beta$ -actin antibodies. WT: oocytes injected with wt-HCN2 mRNA, NI: non-injected oocytes; L377H, P493L and G587D: oocytes injected with p.(Leu377His), p.(Pro493Leu) and p.(Gly587Asp) variants mRNAs, respectively. (G-J) Study of membrane trafficking of p.(Leu377His), p.(Pro493Leu) and p.(Gly587Asp) variants in HEK293 cells. The expression of EGFP-tagged p.(Leu377His) or p.(Pro493Leu) or p.(Gly587Asp) HCN2 variants was evaluated by confocal microscopy. The cells were stained with the CellMask orange membrane stain and DAPI nuclear stain. EGFP-tagged wt-HCN2 (G, left panel) shows a strong EGFP signal at the plasma membrane, while the trafficking-defected HCN2 $_{\Delta C-X}$  (Thr553Ter) shows cytosolic staining (G, right panel), as seen for p.(Leu377His), p.(Pro493Leu) and p.(Gly587Asp) variants (H-J). Examples of images obtained from magnification of 63x are shown (G and H-J, left panels). Examples of overview with magnification from 20x are also shown (H-J, right panels).

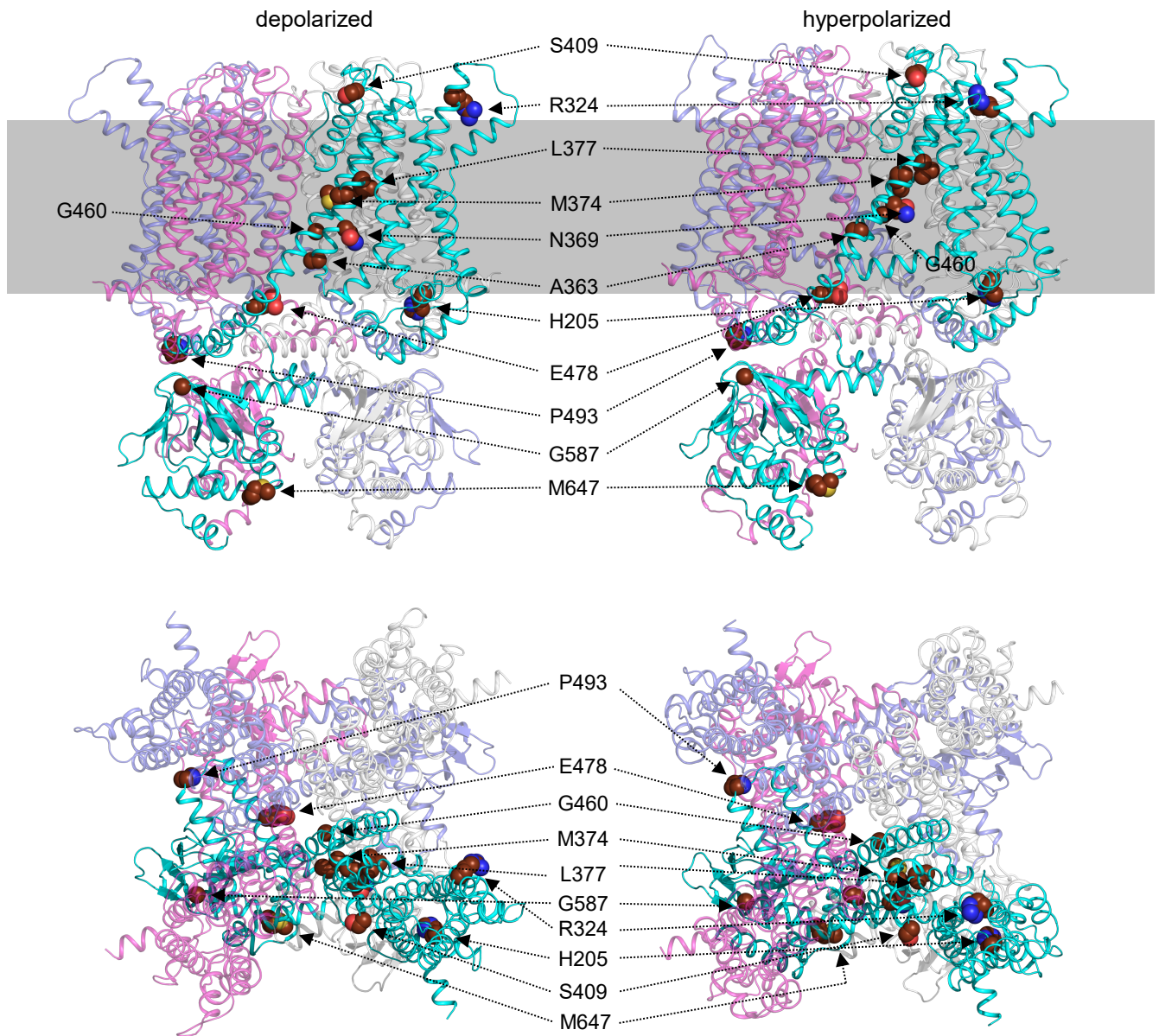


**Figure 5 Mutation mapping onto 3-dimensional homology models of HCN2 in depolarised and hyperpolarised states.** Models of HCN2 in depolarized (left panels) and hyperpolarized states (right panels) are shown (upper panels: profile views, lower panels: top views). Proteins are drawn in ribbon representation with a different color code for each subunit. For clarity, the locations of mutated amino acids are represented as spheres in only one subunit (in cyan), while the other subunits are shown in semi-transparent representations. The approximate position of HCN2 within the membrane is visualized with the gray rectangle (profile views).

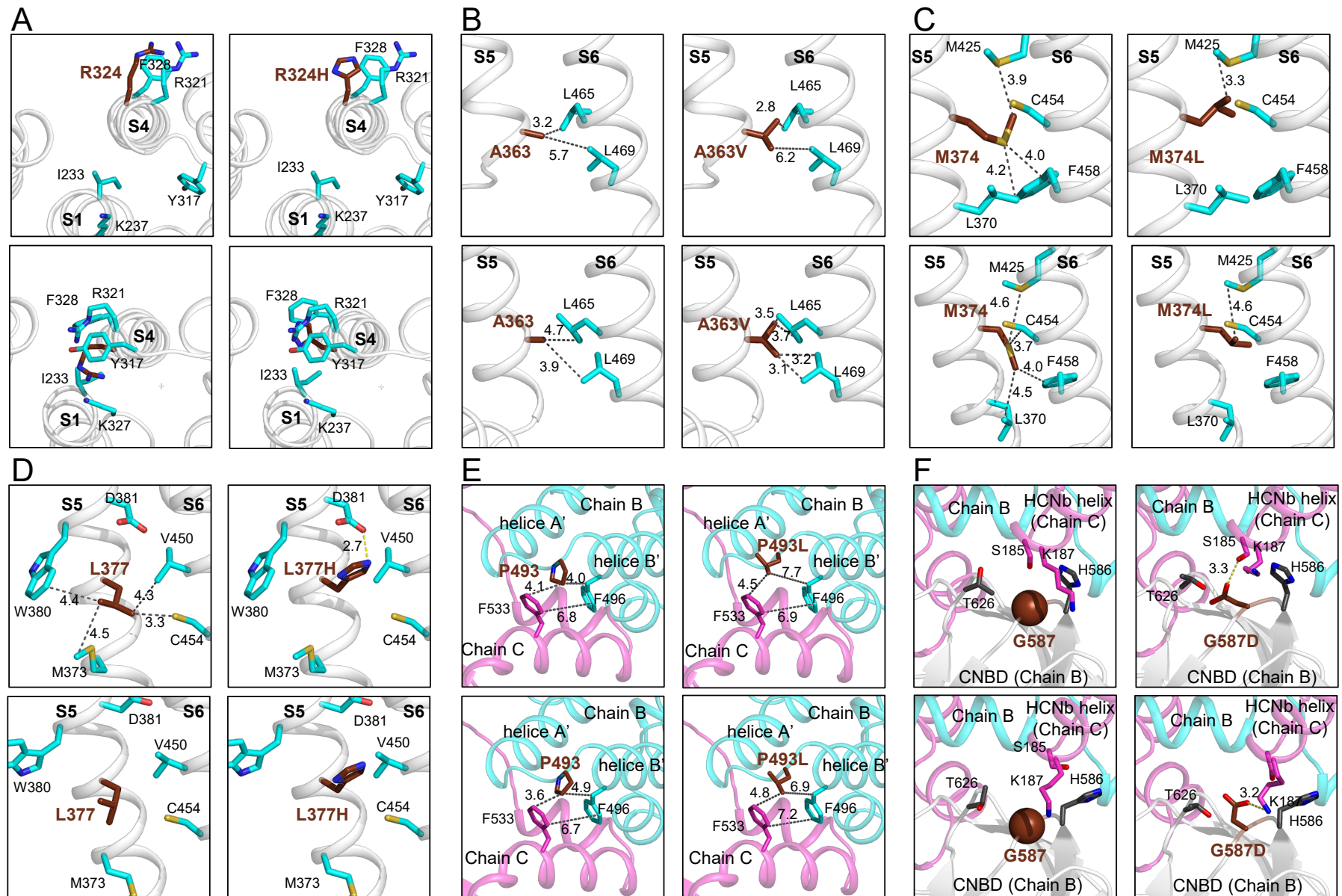


**Figure 6 Structural analysis of p.(Arg324His), p.(Ala363Val), p.(M374Leu), p.(Leu377His), p.(Pro493Leu) and p.(Gly587Asp) HCN2 variants.** For clarity, zoom in of profile views were chosen for each variant, except for p.(Arg324His) variant. **(A)** Top view of S1-S4 helices of wt-HCN2 and p.(Arg324His) variant in the depolarized and hyperpolarized states. The side chain of residue at 324 is towards the solvent in the depolarized state of HCN2 (left panel), but after opening it becomes buried in a hydrophobic pocket formed by I233, L323, Y317, F328, M390 and L391. **(B, C and D)** Profile views of S5-S6 interfaces showing the residues A363 **(B)**, M374 **(C)** and L377 **(D)**. **(E and F)** The p.(Pro493Leu) and p.(Gly587Asp) variants are concerned the intracellular C-termini of HCN2, at the interface between two subunits (Chains B and C). The p.(Pro493Leu) variant **(E)** might destabilize the bend between helices A' and B' and also the N-terminal of helix B'. The p.(Gly587Asp) variant could change the curvature of the loop between two  $\beta$ -sheets within the CNBD **(F)**. The proteins are drawn in ribbon representation, and their closest-neighbour contacts with residues of S6. The distances are indicated in Å.